

Entropic force of cone-tethered polymers interacting with a planar surface

James M. Polson^{1, a)} and Roland G. MacLennan¹

Department of Physics, University of Prince Edward Island, 550 University Avenue, Charlottetown, Prince Edward Island, C1A 4P3, Canada

Computer simulations are used to characterize the entropic force of one or more polymers tethered to the tip of a hard conical object that interact with a nearby hard flat surface. Pruned-enriched-Rosenbluth-method (PERM) Monte Carlo simulations are used to calculate the variation of the conformational free energy, F , of a hard-sphere polymer with respect to cone-tip-to-surface distance, h , from which the variation of the entropic force, $f \equiv |dF/dh|$, with h is determined. We consider the following cases: (1) a single freely-jointed tethered chain, (2) a single semiflexible tethered chain, and (3) several freely-jointed chains of equal length each tethered to the cone tip. The simulation results are used to test the validity of a prediction by Maghrebi *et al.* (EPL, **96**, 66002(2011); Phys. Rev. E **86**, 061801 (2012)) that $f \propto (\gamma_\infty - \gamma_0)h^{-1}$, where γ_0 and γ_∞ are universal scaling exponents for the partition function of the tethered polymer for $h = 0$ and $h = \infty$, respectively. The measured functions $f(h)$ are generally consistent with the predictions, with small quantitative discrepancies arising from the approximations employed in the theory. In the case of multiple tethered polymers, the entropic force per polymer is roughly constant, which is qualitatively inconsistent with the predictions.

I. INTRODUCTION

Confinement of a polymer chain to a sufficiently small space distorts its shape, leading to a significant reduction in its conformational entropy and thus an increase in its free energy. The effects of confinement on single-polymer conformational statistics has been the subject of numerous theoretical and computational studies, which have examined variety of confinement geometries, including cavities,¹⁻⁴ channels,⁵⁻⁹ slits,¹⁰⁻¹⁴ as well as more complex geometries.^{15,16} Most relevant to the present work is the case of a polymer confined to a slit between two parallel hard walls.¹¹⁻¹⁴ These studies have characterized the scaling of the molecular dimensions and free energy with respect to confinement dimension, contour length and persistence length. Distinct scaling regimes such as the de Gennes, extended de Gennes and Odijk regimes have been identified, and some predictions have been verified by experiments employing fluorescently labeled DNA molecules confined to nanoslits.¹⁷

A system conceptually similar to that of a slit-confined polymer was examined a number of years ago Maghrebi *et al.*^{18,19} In these studies, a polymer was confined to the space between a flat surface and a hard cone, with one end of the polymer tethered to the tip of the cone. The system is illustrated in Fig. 1. Note that this reduces to a slit-confined tethered polymer when the cone angle α (defined in the figure) is 90° . As is the case for confinement between parallel walls, the conformational free energy increases upon a reduction in the distance between the surfaces, here defined as the cone-tip-to-surface distance, h . Remarkably, the entropic force, $f \equiv |dF/dh|$, is expected to satisfy the simple universal relation, $f = \mathcal{A}k_B T/h$, where k_B is Boltzmann's constant and T is absolute temperature. The relation is expected to hold for sufficiently

long chains in the regime where $a \ll h \ll R_g$, where a is the link length (monomer size or persistence length) and R_g is the root-mean-square radius of gyration of a free polymer. The proportionality constant, \mathcal{A} , depends solely on basic geometrical factors and gross features of the polymer and is of the order of unity. The scaling relation also holds more generally for other systems provided the two obstructing surfaces are scale invariant. (Other examples include pyramids and wedges.) Maghrebi *et al.* calculated \mathcal{A} for both ideal and real (i.e., self-avoiding) polymers using analytical, simulation, and ϵ -expansion methods. The ϵ -expansion was also used to estimate the effects of multiple polymers tethered to the cone tip on the entropic force.

The theoretical analysis of the tethered-polymer system examined in Refs. 18 and 19 was intended to provide motivation for future experimental measurements of entropic forces of polymers using atomic force microscopy (AFM). In this scenario, the cone represents the AFM cantilever tip, at the end of which is attached one or more polymers. As the prefactor \mathcal{A} is expected to be of order unity, the measured force for a single tethered polymer at room temperature is predicted to be of order 0.1 pN for a distance of order 0.1 μm , which they noted was just at the margins of measurement for precision AFM devices. On the other hand, the authors also noted that using multiple polymers tethered to the AFM tip would increase the magnitude of the force without changing the form of the force-distance relation. Recently, such experiments were carried out by Liu *et al.*, who measured the entropic force of polyethylene glycol (PEG) polymers tethered to pyramidal cantilever tip in the vicinity of a flat surface.²⁰ The measurements were made in salt water solution to minimize the effects of electrostatic forces and a hydrophobic plate to minimize polymer adhesion forces. Force-distance curves were measured and compared to the prediction of Maghrebi *et al.*, as well as to the Alexander-de Gennes (AdG) theory for a polymer brush.²¹ Each analysis suggested that a few tens of poly-

^{a)}Electronic mail: jpolson@upe.ca

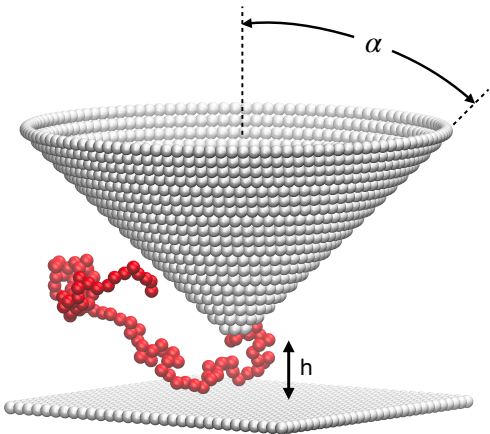


FIG. 1. Illustration of the system examined in this study. A polymer is tethered to the tip of a hard conical object in the vicinity of hard planar surface. The cone and the surface both extend to infinity. The cone half-angle, α , and the cone-tip-to-surface distance, h , are both illustrated. We examine cases of single flexible and semiflexible chains as well as multiple flexible chains tethered to the cone tip.

mers had been tethered to the cantilever. Notably, the AdG theory appeared to provide a more accurate prediction, calling into question either the relevance of the theory of Maghrebi *et al.* to such experiments or else the appropriateness of the design of this particular experiment to test the theory.

The purpose of the present study is to use computer simulations to examine the accuracy of the prediction for the force-distance relation, $f = \mathcal{A}k_B T/h$. As noted above, the relation is expected to hold only for polymers that are sufficiently long and only over a restricted range of h where that distance is the only relevant length scale. Systems for which these conditions are only marginally satisfied are expected to show deviations from the predictions, and a key goal of the study is to quantify such effects. The calculations can be used to determine the origin of the discrepancy between theory and the experiments of Ref. 20 and to provide insight for use in future experiments that can be designed to provide a more meaningful test of the theory. The other goal of the study is more fundamental. In their first study on this topic,¹⁸ Maghrebi *et al.* write: “The simple force law... follows easily from various polymer scaling forms... and should be part of polymer lore. Surprisingly, we could not find an explicit reference to it in any of the standard polymer textbooks.” Over recent decades, computer simulation methods have provided valuable insight into the many other scaling predictions in polymer physics that do appear in the standard texts, and the present work should help address the omission noted by the authors.

The remainder of the article is organized as follows. In Sec. II, we review the derivation of the prediction for

the force-distance relation, highlighting the various approximations that are employed. In Sec. III, we briefly describe the simple molecular model used in the simulations. Section IV outlines the MC simulation methods that were employed for the calculations. Section V presents the results for three variations of the model polymer: (1) a single tethered flexible chain, (2) a single tethered semiflexible polymer, and (3) multiple tethered flexible chains. Finally, in Sec. VI we summarize the key findings of the study.

II. THEORY

In this section we provide a brief review of the derivation of the force-distance relation for the cone-tethered polymer system first presented by Maghrebi *et al.*,^{18,19} highlighting the various approximations that are employed in the process.

Consider a single self-avoiding polymer chain tethered to the apex of a hard cone of half-angle α . The tip of the cone, and thus the tethered monomer, is located a distance h from an infinite, hard flat surface, whose normal is aligned with the symmetry axis of the cone. The system is illustrated in Fig. 1. The special cases of $h = 0$ and $h = \infty$ correspond to scale-free confinement geometries. (Note: In this article, $h = \infty$ is used to denote the case of no polymer-plane interactions for polymers of arbitrary length.) In such cases, the partition function for a self-avoiding polymer has the form²¹

$$Z = bq^N N^{\gamma-1}, \quad (1)$$

where q is the effective coordination number of the polymer, b is a model dependent coefficient of order unity whose value depends on h (i.e., $h = 0$ or $h = \infty$), and γ is a universal exponent that depends on the cone angle α . Since the conformational free energy of the polymer is given by $F/k_B T = -\ln Z$, the free energy difference between the systems for $h = 0$ and $h = \infty$ is given by

$$\Delta F/k_B T = C + \Delta\gamma \ln N, \quad (2)$$

where $\Delta F \equiv F_0 - F_\infty$, $C \equiv -\ln(b_0/b_\infty)$ and $\Delta\gamma \equiv \gamma_\infty - \gamma_0$, and where the subscripts refer to the cases of $h=0$ and $h=\infty$.

Now consider the case of arbitrary tip-to-surface distance h . As h decreases and the cone comes closer to the flat surface, the polymer becomes increasingly confined, and thus its conformational entropy decreases. This in turn effects an increase in the free energy, F . The magnitude of the entropic force, defined as $f \equiv |dF/dh|$, is also expected to increase with a reduction in h . Using dimensional analysis, Maghrebi *et al.* have argued that the entropic force should vary inversely with h ,

$$f = \mathcal{A} \frac{k_B T}{h}, \quad (3)$$

in the regime where $a \ll h \ll R_g$, where a is the size of a link in the polymer chain (i.e. the monomer width for a

freely-jointed chain model and the persistence length in the case of a semiflexible polymer), and R_g is the root-mean-square radius of gyration of a free polymer. This scaling ansatz follows from the fact that h is the only relevant length scale in this regime. The quantity \mathcal{A} depends only on geometric factors, such as the cone angle. They estimate \mathcal{A} as follows. The work done against the entropic force in bringing the cone from far away to make contact with the plate is calculated:

$$W = \int_a^{R_g} dh f(h) = \mathcal{A} k_B T \ln \left(\frac{R_g}{a} \right). \quad (4)$$

The upper bound on the integral arises from the fact that $f \approx 0$ until $h \approx R_g$ and the lower bound is due to the fact that f is too large for the cone to approach the surface at distances below a . The radius of gyration scales as $R_g/a = cN^\nu$, where N is the number of polymer links and where $\nu \approx 0.588$ for a self-avoiding polymer.²² The scaling prefactor, c , is of order unity and depends on the details of the molecular model. Substitution into Eq. (4) yields: $W = \mathcal{A} \nu k_B T \ln(N) + \mathcal{A} \nu k_B T \ln(c)$. Since c is of order unity, we can neglect the second term, which gives

$$W = \mathcal{A} \nu k_B T \ln(N). \quad (5)$$

The work done against the entropic force is simply equal to ΔF , the change in the free energy in moving the cone from far away to a point where it is in contact with the surface. Comparing Eq. (2) (but ignoring the additive constant C) and Eq. (5), it follows: $\mathcal{A} = \Delta\gamma/\nu$, where $\Delta\gamma \equiv \gamma_\infty - \gamma_0$. Consequently,

$$f = \frac{\Delta\gamma k_B T}{\nu h}. \quad (6)$$

Equation (6) thus predicts that the entropic force scales inversely with the tip-to-surface distance h . The proportionality factor $\Delta\gamma$ depends on the cone angle α . As α increases, the degree of confinement also increases. This will result in a reduction in conformational entropy and an expected increase the entropic force. Thus, $\Delta\gamma$ is expected to increase monotonically with increasing α . Note that f is independent of the polymer length N as well as the persistence length. Thus, the functions $f(h)$ for different values of N and κ are expected to overlap in the regime where the condition $a \ll h \ll R_g(N)$ is satisfied for each polymer chain. A key goal of the present study is to test the validity of the prediction in Eq. (6).

III. MODEL

We employ a very simple, athermal model in our simulations. The model consists of one or more polymer chains tethered to the tip of a hard, conical object in the vicinity of a hard, flat surface whose normal is parallel to the symmetry axis of the cone. In all cases, the polymer is modeled as a chain of $N + 1$ hard spheres, with sphere diameter and fixed bond length both equal

to σ , which defines the length scale. We consider the cases of both a freely-jointed chain and a semiflexible chain. In the latter case, the bending rigidity of the polymer is modeled using a bending potential with the form, $u_{\text{bend}}(\theta) = \kappa(1 - \cos\theta)$. The angle θ is defined for a consecutive triplet of monomers centered at monomer i such that $\cos\theta_i = \hat{u}_i \cdot \hat{u}_{i+1}$, where \hat{u}_i is the unit vector pointing from monomer $i - 1$ to monomer i . The bending constant κ determines the overall stiffness of the polymer and is related to the persistence length P by²³ $\exp(-\langle l_{\text{bond}} \rangle / P) = \coth(\kappa/k_B T) - k_B T / \kappa$, where $\langle l_{\text{bond}} \rangle$ is the mean bond length. For our model, the bond length is fixed to $l_{\text{bond}} = \sigma$. Note that for sufficiently large $\kappa/k_B T \gg 1$ this implies $P/\sigma \approx \kappa/k_B T$.

The polymer is tethered to the tip of a hard conical structure of half-angle α . The center of the first monomer is located at the exact tip of the cone. The cone-tip-to-surface distance h is defined such that $h = 0$ corresponds to the tethered monomer being in contact with the surface. Configurations in which monomers overlap with each other, the cone, or with the surface have an energy of infinity and thus are forbidden. For the case of multiple tethered polymers, each polymer shares the same end monomer that is tethered to the cone tip. All simulations for multiple-polymer systems used only the freely-jointed chain model.

IV. METHODS

We use Pruned-enriched Rosenbluth method (PERM) simulations to calculate the excess free energy of the tethered polymer. PERM is a chain growth MC method that uses a dynamic bias to obtain importance sampling. PERM is based on the Rosenbluth-Rosenbluth (RR) method, which can also be used to calculate polymer free energies. PERM uses a more sophisticated algorithm that enables it to overcome the well known attrition problem that limits the applicability of the RR method to rather short polymers of $\mathcal{O}(10^2)$ segments. By contrast, PERM can be used to grow polymer chains orders of magnitude greater in length. In this algorithm, a tree of chains, called a ‘‘tour’’, is grown using the operations of ‘‘pruning’’ and ‘‘enriching’’ in such a way as to dramatically reduce the attrition rate of the RR method.

We employ an off-lattice version of the algorithm developed by Tree *et al.*²⁴ The initial monomer is placed at the tip of the cone and for the n th growth step a set of K trial steps are calculated. For freely-jointed chains, the orientation of the trial monomer position is chosen with equal probability for all directions. For semiflexible chains, the orientations are drawn from a probability distribution governed by the bending potential, u_{bend} . Each trial step is assigned a Rosenbluth weight

$$a_n^{(k)} = \exp(-U_n^{(k)}/k_B T). \quad (7)$$

Here, $U_n^{(k)}$ is the potential energy associated with the k th trial placement of monomer n . It includes non-bonded

interactions with previously grown monomers (i.e. those with index $< n$), as well as monomer-wall interactions. Note that these interactions are athermal in character, i.e., the energy is infinity if a monomer overlaps with another monomer or with a confining wall and is zero otherwise. Thus, $a_n^{(k)} = 1$ if the trial move does not result in overlap and $a_n^{(k)} = 0$ if it does result in overlap. The weight of the n th growth step is defined

$$w_n = \sum_{k=1}^K a_n^{(k)}. \quad (8)$$

Clearly, w_n is an integer in the range $w \in [0, K]$ and is a count of the number of trial moves that do not result in overlap. To make one step, one of the trial steps is randomly chosen according to the probability

$$p_n^{(k)} = a_n^{(k)} / w_n. \quad (9)$$

The cumulative weight of the n th chain step is defined:

$$W_n = \prod_{i=0}^n w_i. \quad (10)$$

This is an approximate count of the number of configurations generated using K trial moves per step.

In principle, the average of W_n can be used to calculate the excess free energy of the polymer, $F_{\text{ex}}(n)$,

$$\beta F_{\text{ex}}(n) = -\ln \left(\frac{Z_n}{Z_{\text{id},n}} \right) \approx -\ln \langle W_n \rangle \quad (11)$$

where

$$F_{\text{ex}}(N, h; \alpha) \equiv F(N, h; \alpha) - F_{\text{id}}(N), \quad (12)$$

where $\beta F = -\ln Z$ is the total conformational free energy of the polymer chain with configurational partition function Z , and where $\beta F_{\text{id}} = -\ln Z_{\text{id}}$ is the free energy of an ideal chain (i.e., in the absence of all monomer-monomer and monomer-wall interactions) with partition function Z_{id} . While both F and F_{id} depend on chain length N , F (and therefore F_{ex}) also depends on the parameters associated with the confining geometry, h and α . As the chain grows, W_n fluctuates and very quickly can approach zero if no trial positions can be found that do not lead to monomer-monomer or monomer-wall overlap, thus leading to the problem of attrition mentioned above. To overcome this problem, PERM uses the procedures of pruning and enrichment to bias the chain growth toward successful states, i.e., those without any overlap. In cases where W_n rises above its ensemble average $\langle W_n \rangle$, chain growth is taken to be successful, and the tour is “enriched” by spawning branches, or copies. If $W_n / \langle W_n \rangle$ falls then chain growth is struggling, and the tour is terminated along this branch, i.e. it is “pruned”. The pruning rate and the number of copies created during enrichment are determined by the ratio, $W_n / \langle W_n \rangle$, using the stochastic, parameterless procedure described by Prellberg and Krawczyk.²⁵ The continuous pruning

and regrowing of the chain leads to a depth-first type of diffusion along the chain contour length.²⁶

In Eq. (11), we note that the desired quantity, $F_{\text{ex}}(n)$ depends on the average $\langle W_n \rangle$, which itself is used in the criterion for choosing to prune or enrich the chain during execution of the growth process in the simulation. While $\langle W_n \rangle$ can be estimated during run-time and used to calculate a more accurate estimate in a self-consistent calculation, initial estimates can be poor, leading to a slow execution, particularly for longer chains. To overcome this problem, we conduct a sequence of short runs to find an approximate estimate for $\langle W_n \rangle$. We then carry out a single long run using the estimate to determine the pruning and enrichment probabilities in order to determine a much more accurate value of $\langle W_n \rangle$ and, therefore, F_{ex} . These short runs are carried out as follows. We first grow a chain of length N_{inc} monomers using the RR method and calculate the $\langle W_n \rangle$ for $n \in [1, N_{\text{inc}}]$. Then we grow a chain of length $2N_{\text{inc}}$, using PERM with the previous estimate of $\langle W_n \rangle$ to grow the first N_{inc} monomers and the RR method to grow the next N_{inc} monomers. This yields an estimate of $\langle W_n \rangle$ in the range $n \in [0, 2N_{\text{inc}}]$. This process is applied iteratively for N/N_{inc} steps until a chain of length N is grown and $\langle W_n \rangle$ is estimated for the full range of chain lengths. In a typical run for a polymer of length $N=5000$ using $K=10$ trial steps used $N_{\text{inc}}=100$ and thus $N/N_{\text{inc}}=50$ increments with each simulation using 10^5 tours, and the final run used 10^6 tours. To maximize computational efficiency, we employ the neighborlist method described in the Supporting Information for Ref. 24.

A system with multiple polymers tethered to the cone tip can also be thought of as a star polymer with the same number of “arms” and with the branch point tethered to the tip. Modification of the algorithm for use with star polymers is straightforward and has been described previously.²⁷⁻²⁹ The most important detail is that each arm of the polymer is essentially grown together simultaneously. To illustrate, consider a star polymer with arms that are currently all of the same length. One monomer is added to the first arm, the next monomer is added to the second arm, and so on, until all arms are again of the same length, following which the cycle begins again. In this study, we consider systems of up to $n_{\text{arm}} = 5$ arms each of length up to $N = 1000$ monomers.

PERM simulations were used to calculate the excess free energy, $F_{\text{ex}}(N, h; \alpha)$, for single tethered polymers up to a length of $N=5000$ segments for cone-tip-to-surface distances in the range $h \in [0, 300\sigma]$ in integer increments of σ for freely-jointed chains and $h \in [0, 400\sigma]$ for semiflexible chains. For star-polymer (i.e., multiple-chain) systems, we examined up to $n_{\text{arm}} = 5$ arms, each of length up to $N = 1000$ monomers. In addition, we use cone angles in the range $\alpha \in [10^\circ, 90^\circ]$. The entropic force, $f \equiv |dF/dh| = |dF_{\text{ex}}/dh|$ was calculated by first fitting $F_{\text{ex}}(h)$ to a function typically of the form, $F = \exp(\sum_{n=0}^5 a_n (\ln(x+2))^n) + a_6$, by adjustment of the parameters $\{a_n\}$. This provided an excellent fit of

the function over the full range of h . Subsequently, $f(h)$ was determined from an analytical derivative of the fitting function. Typically, f exhibited power-law scaling with respect to h over an intermediate range of h . A fit of the calculated $f(h)$ in this range yields an estimate of the scaling exponent. In cases where the uncertainty in the scaling exponent was desired, a second analysis method was employed. First, a simple finite-difference method was used to estimate the derivative dF/dh over this range. A fit of these data then yielded an estimate of the scaling exponent, which was typically very close to that obtained using the first method, as well as an estimate of the uncertainty.

In the results presented below, distances are measured in units of the monomer diameter, σ , and energy is measured in units of $k_B T$.

V. RESULTS

A. A single tethered freely-jointed chain

PERM simulations were used to calculate the excess free energy, defined in Eq. (12), of a single self-avoiding freely-jointed hard-sphere chain tethered to the tip of a hard cone located a distance h from a hard flat surface. We define the free energy difference

$$\begin{aligned} \Delta F &\equiv F(N, 0; \alpha) - F(N, \infty; \alpha) \\ &= F_{\text{ex}}(N, 0; \alpha) - F_{\text{ex}}(N, \infty; \alpha) \end{aligned} \quad (13)$$

where $h = 0$ corresponds to the tethered monomer in contact with the surface and $h = \infty$ effectively corresponds to a simulation in the absence of the flat surface. Thus, the difference in the excess free energy measured in the two simulations with $h = 0$ and $h = \infty$ yields the difference in the total conformational free energy that appears in Eq. (2). Consequently, the measured difference in the excess free energy obtained from the two PERM simulations should scale linearly with $\ln(N)$, with a proportionality constant of $\Delta\gamma \equiv \gamma_\infty - \gamma_0$.

Figure 2(a) shows the variation of ΔF with N for systems with several values of α . As expected, ΔF varies linearly with $\ln(N)$ for sufficiently long chains. The dashed lines show fits to the data in the region $N \in [150, 5000]$. The fitted curves are extended to the range $N < 150$ to highlight the expected discrepancy between the fit and the free energy in the low- N regime. The fits yield values of $\Delta\gamma$ for each cone angle, and the results are plotted in Fig. 2(b). As expected, $\Delta\gamma$ increases monotonically with increasing cone angle α as a result of increasing confinement and a corresponding loss of conformational entropy. The variation of $\Delta\gamma$ with α appears to be consistent with that measured by Maghrebi *et al.*^{18,19} In that study the excess free energy was calculated using a different method and for a lattice-model polymer system. In the limit of very large N the two results are expected to converge.

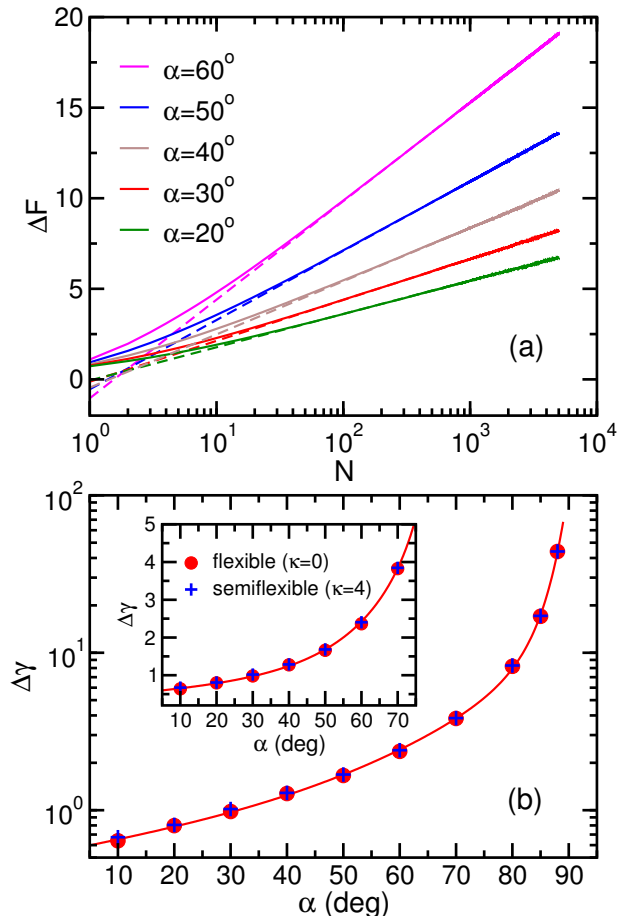


FIG. 2. (a) Free energy difference $\Delta F \equiv F(h = 0) - F(h = \infty)$ vs polymer length N for a single freely-jointed chain tethered to a cone of half-angle α . Results for various values of α are shown. The dashed lines show fits of the data in the region $N \in [150, 5000]$ to the function $\Delta F = a_0 + a_1 \ln N$. The fitted curves extend to lower values of N to highlight the discrepancy in this region. (b) Variation of $\Delta\gamma$ with α , where $\Delta\gamma \equiv \gamma_\infty - \gamma_0$ was obtained from the fits of the data in panel (a). The inset shows a close up of the data for low α plotted using a linear scale for $\Delta\gamma$. The solid line is a guide for the eye. Overlaid on these results are data for semiflexible chains with $\kappa=4$ for calculations described in Sec. VB. Note that the uncertainties in the data points are smaller than the size of the symbols.

Next, we consider the variation of the free energy, F , with the distance h . Note from Eq. (12) that $F(h)$ differs from F_{ex} , the quantity actually calculated in the simulations, by a constant amount F_0 , the free energy of a free, ideal polymer. It is convenient to redefine $F(h)$, such that $F \rightarrow 0$ in the limit where h is large, effectively by adding another constant. Figure 3 shows the variation of F with h for a cone angle of $\alpha = 50^\circ$ and for various polymer lengths. The free energy was calculated for tip-to-surface distances in the range $h = 0 - 300$, where the

upper bound was chosen to be sufficiently large that F has decayed to its large- h limit by this point. The inset shows the corresponding variation of the entropic force with h . The curves overlap at small h , but eventually diverge as h increases. In the overlap region, f obeys a power law. As h increases, each curve eventually peels away from this power-law curve, with shorter chains diverging before longer ones. The divergence arises from the violation of the condition that $h \ll R_g$ required for the validity of Eq. (6), which predicts $f(h)$ to be independent of N . Shorter chains violate the condition before longer ones upon increasing h . Somewhat surprisingly, the curves largely overlap and maintain the same power-law scaling right down to $h = 1$, thus violating the previously stated condition that $a \ll h$ (here, $a=1$ is the monomer size) is required for the validity of the theoretical prediction. Presumably, this condition is of lesser importance than $h \ll R_g$.

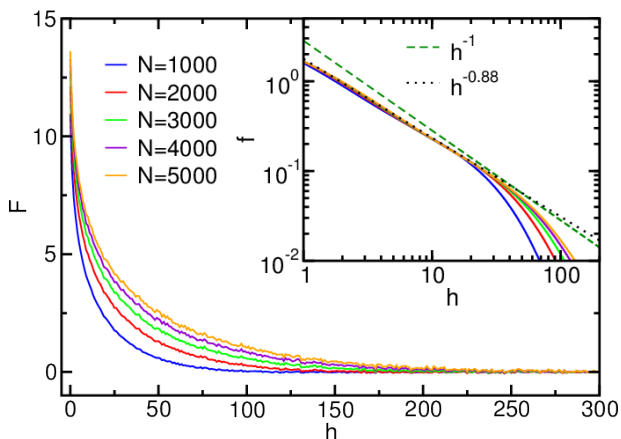


FIG. 3. Free energy F vs tip-to-surface distance h for a cone angle of $\alpha = 50^\circ$. Results for various polymer lengths are shown. The inset shows the variation of the entropic force, $f \equiv |dF/dh|$, with h . The green dashed line shows the theoretical prediction using the value of $\Delta\gamma$ for $\alpha = 50^\circ$ in Fig. 2(b). The dotted black line shows a fit of the $N = 5000$ curve to the function $f = cN^\mu$ in the region $h \in [4, 20]$.

To estimate the scaling exponent for $N = 5000$ a finite-difference method was used to estimate the force in the range $h \in [4, 30]$, and a subsequent fit to a power-law function yields scaling exponent of -0.88 ± 0.08 . The fitted curve is qualitatively consistent with the theoretical curve calculated using the value of $\Delta\gamma$ obtained from Fig. 2. However, the quantitative discrepancy is notable. The theory predicts an entropic force that is somewhat larger than the measured values. In addition, the scaling exponent is close to, but somewhat smaller than the predicted value of -1 .

Figure 4 shows the variation of F with h for a $N=5000$ polymer tethered to a cone with several different values of α . As in Fig. 3, these results are used to calculate

the variation of the entropic force f with h . Those results are shown in the inset of the figure. As in Fig. 3, there is a range of h over which f varies approximately inversely with h . Again, however, the measured exponent of -0.88 is somewhat smaller in magnitude than the predicted value. For comparison, a curve with the predicted exponent of -1 is overlaid on the graph. As before, the discrepancy between theory and simulation likely arises from the approximations employed in the derivation of Eq. (6). Note that $f(h)$ increases with increasing α . This is consistent with the prediction that the scaling prefactor of Eq. (6) is proportional to $\Delta\gamma$ and the fact that $\Delta\gamma$ increases with α , as illustrated in Fig. 2(b).

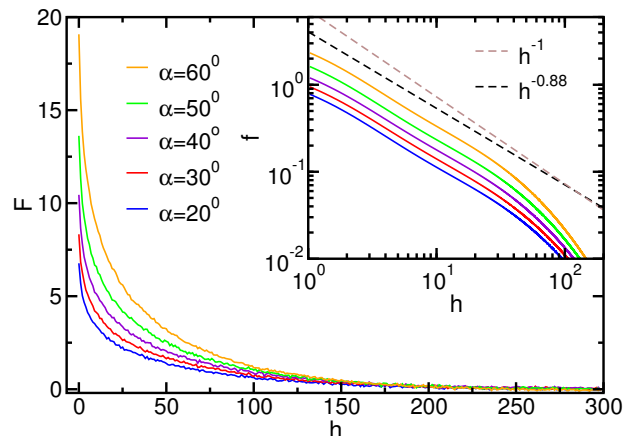


FIG. 4. Free energy F vs tip-to-surface distance h for a polymer of length $N=5000$. Results for different cone angles are shown. The inset shows the variation of the entropic force, $f \equiv |dF/dh|$, with h . The dashed lines show the functions proportional to $h^{-0.88}$ and h^{-1} .

Figure 5 shows the variation of f with the $\Delta\gamma$ using the data from the inset of Fig. 4 for a cone tip-to-surface distance value of $h = 10$, as well as the values of $\Delta\gamma$ obtained from the data of Fig. 2. This value of h lies in the region where f exhibits the power-law dependence on h and marginally satisfies the condition $a \ll h \ll R_g$ required for the prediction of Eq. (6) to be valid. Equation (6) predicts that f varies linearly with $\Delta\gamma$ with a slope of $1/(\nu h) = 0.1700$, shown as the blue curve in the figure. By contrast, the simulation data yields a linear dependence, but with a slope of 0.141 . Once again, the approximations employed in the derivation of Eq. (6) lead to small but significant quantitative discrepancies with the simulation results.

In the limit $\alpha \rightarrow 90^\circ$, the cone becomes a plane, and thus the polymer is confined to the space between two parallel surfaces. This system has been the subject of numerous studies in recent decades, and the dependence of the conformational free energy on inter-plane spacing and polymer length is well characterized for both flexible and semi-flexible chains. In the case of flexible

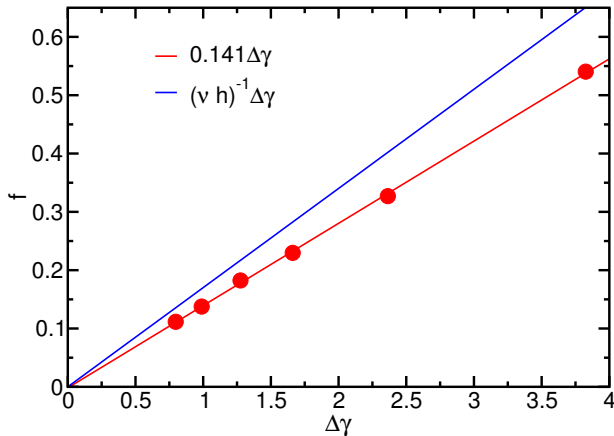


FIG. 5. Entropic force f vs $\Delta\gamma$ for $N=5000$ and $h=10$ obtained from the data of the inset of Fig. 4. The red line is a linear fit with a slope of 0.141. The blue curve is the prediction using Eq. (6) using $h = 10$ and $\nu = 0.588$. The uncertainties in the data points are smaller than the symbol size.

chains in the de Gennes regime, where $a \ll h \ll R_g$ (for monomer size a), the confinement free energy is equal to the number of thermal blobs, which leads to the scaling $F \sim Nh^{-1/\nu} \approx Nh^{-1.7}$, for $\nu \approx 0.588$. This yields an entropic force of $f \equiv |dF/dh| \sim Nh^{-1/\nu-1} \approx Nh^{-2.7}$. The scaling exponent of -2.7 is significantly different from the value of -1 predicted from Eq. (6). Note that the fact that the chain is tethered to a point on the plane (i.e. the $\alpha = 90^\circ$ “cone”) is only expected to have a tiny effect on $F(h)$ and so does not explain the discrepancy.³⁰ Evidently, there is a regime scale crossover as α increases that is not accounted for in the derivation of Eq. (6).

To elucidate this crossover, we show the variation of $F(h)$ with cone angle in the range $\alpha \in [60^\circ, 90^\circ]$ in Fig. 6(a). For the case of confinement to a slit ($\alpha = 90^\circ$), the de Gennes-regime scaling of $F \sim h^{-1.7}$ is observed for intermediate values of h . At large h , the power-law exponent increases. The curves for all cone angles converge in the limit of large h . As the distance h decreases, the curves for $\alpha < 90^\circ$ diverge from the $\alpha = 90^\circ$ curve. Unsurprisingly, a free energy curve hugs more closely to the $\alpha = 90^\circ$ curve the greater the cone angle. Figure 6(b) shows the variation of the entropic force f with h calculated using the data of Fig. 6(a). The crossover between the predicted power-law scaling for slit confinement in the de Gennes regime ($f \sim h^{-1/\nu-1} \approx h^{-2.7}$) to the scaling close to that predicted in Eq. (6) (i.e., $f \sim h^{-0.88}$ rather than $f \sim h^{-1}$) with increasing α is clearly illustrated. Note that the range of h for which the latter scaling regime holds decreases as the cone becomes sharper, i.e., as α decreases.

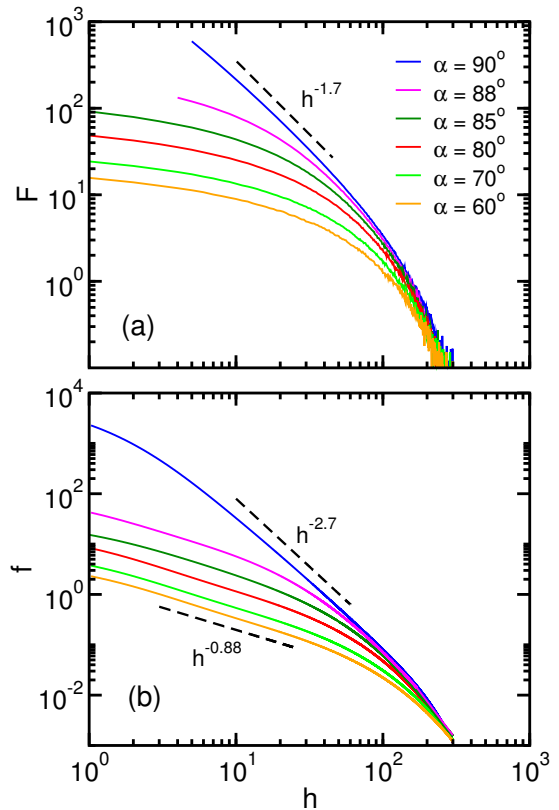


FIG. 6. (a) Free energy vs cone-tip-to-surface distance h for a polymer of length $N=5000$ tethered to a cone. Values for various values of α are shown. The dashed line is the predicted power-law scaling for slit confinement in the de Gennes regime. (b) Entropic force calculated using the data of panel (a). The dashed lines show the prediction for slit confinement in the de Gennes regime ($f \sim h^{-2.7}$) and the observed scaling for $\alpha \lesssim 60^\circ$ noted in Fig. 4 ($f \sim h^{-0.88}$).

B. A single tethered semi-flexible chain

Now we consider the effects of polymer bending rigidity on the entropic force. Figure 7 shows the variation of $\Delta F = F(h=0) - F(h=\infty)$ with N for a chain with a bending rigidity of $\kappa = 4$ tethered to a cone for various values of α . As in Fig. 2(a), the dashed lines show fits to the function $F = a_0 + a_1 \ln(N)$, in this case for $N > 300$, with the fitted line extended to lower N to highlight the expected discrepancy in this regime. The value of a_1 is an estimate of the proportionality factor $\Delta\gamma$ appearing in Eq. (2). As expected, the values of $\Delta\gamma$ are unaffected to the introduction of bending rigidity as they are essentially equal to the values obtained using freely-jointed chains. This is also illustrated clearly for the case of $\kappa=4$, for which the values of $\Delta\gamma$ vs α are overlaid on those for flexible chains in Fig. 2(b). The curves for ΔF vs N for the semiflexible chains differ from those for freely-jointed chains in Fig. 2(a) only by a shift of the

curves to higher free energy. This arises because of the energy required to bend the polymer near the cone tip in the case of $h = 0$, where surface is brought in contact with the cone tip. This shift in ΔF is expected to increase with increasing κ . Note that $\Delta F \approx \kappa$ for $N=1$ for the $\kappa > 0$ curves. This is because the free energy change is dominated by the change in the bending energy associated with the monomer connected to the one fixed at the cone tip. Placing the flat surface at $h=0$ forces the monomer to bend at least 90° , with greater angles discouraged by a still higher bending energy. At this angle, the bending energy is $u_{\text{bend}} = \kappa(1 - \cos(90^\circ)) = \kappa$.

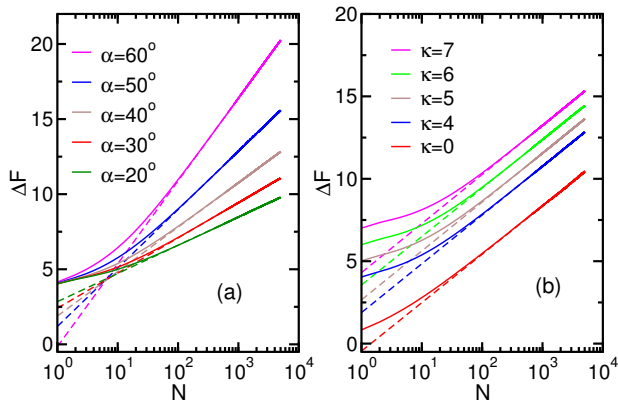


FIG. 7. (a) Free energy difference $\Delta F \equiv F(h=0) - F(h=\infty)$ vs polymer length N for a single semiflexible chain with bending rigidity $\kappa = 4$ tethered to a cone of half-angle α . Results for various values of α are shown. The dashed lines show fits of the data in the region $N \in [300, 2000]$ to the function $\Delta F = a_0 + a_1 \ln N$. (b) As in panel (a), except for fixed cone angle of $\alpha = 40^\circ$ and for various values of κ .

Figure 8 shows the variation of the free energy with h for a semiflexible chain with $\kappa = 4$ tethered to a cone with $\alpha = 40^\circ$. Results for various chain lengths are shown. The inset shows the variation of the corresponding entropic force, f , with h . As for the behavior $f(h)$ for freely jointed chains shown in the inset of Fig. 3, the curves for different N collapse on a single curve for a restricted range of h , which decays with a power law. As h increases further, each curve eventually peels away from the others in the order from shortest to longest. The green dashed curve shows the prediction of Eq. (6), which is a closer match to the simulation data than was the case for the freely-jointed chains. The scaling exponent of the fit to the $N = 5000$ curve in the range $h \in [4, 30]$ is -0.95 ± 0.03 , which is close to the predicted value of -1 .

Figure 9 shows the variation of the entropic force, f , with respect to h for a number of cone angles in the range $\alpha \in [10^\circ, 90^\circ]$. As was the case for flexible chains in Fig. 6(b), the functions exhibit power-law behavior for an intermediate range of h . In the case of slit confinement ($\alpha = 90^\circ$), the scaling exponent in this regime is

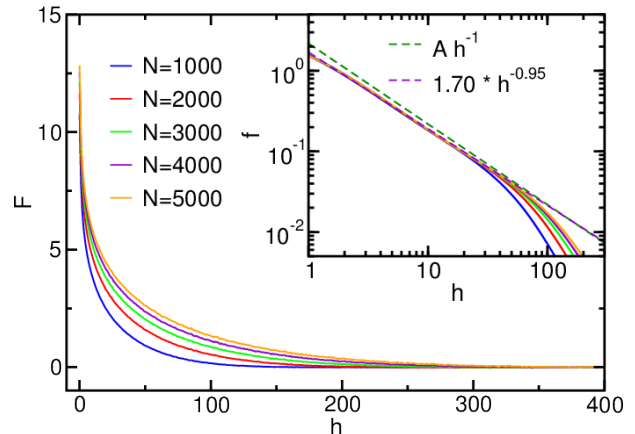


FIG. 8. Free energy F of a semiflexible tethered chain vs tip-to-surface distance h for a cone angle of $\alpha = 40^\circ$. Results for various polymer lengths are shown. The inset shows the variation of the entropic force, $f \equiv |dF/dh|$, with h . The green dashed line shows the theoretical prediction using the value of $\Delta\gamma$ extracted from the fit in Fig. 7. The dotted black line shows a fit of the $N = 5000$ curve to the function $f = cN^\mu$ in the region $h \in [4, 30]$.

consistent with the predictions for the de Gennes regime of $f \sim h^{-1/\nu-1} \approx h^{-2.7}$ for distances roughly in the range $h \in [20, 200]$. (Note that the extended de Gennes regime for slit confinement is present only if the condition $2P < h < 0.2P^2/w$ is satisfied, where P is the persistence length and w is the polymer width.¹³ Noting that $\kappa = 4$ yields $P \approx 4$ and also that $w=1$, the extended de Gennes is not expected to be present for this system.) As the cone angle decreases, the scaling approaches the prediction of Eq. (6) of $f \sim h^{-1}$. The change in the curves as α increases from 10° to 90° is somewhat more complex than the trends for flexible chains evident in the inset of Fig. 4 and in Fig. 6(b).

Figure 10 shows force-distance functions for a polymer of length $N=5000$ tethered to a cone of angle $\alpha = 40^\circ$ for various values of the bending rigidity, κ . Consistent with the prediction of Eq. (6), f is independent of molecular details such as the bending rigidity over an intermediate range of h . At lower and higher values of h , however, the curves diverge slightly. In the case of large h , the force, while very weak, does increase somewhat with increasing κ . This occurs since stiffer chains are expected to stretch somewhat further away from the cone and thus interact more significantly with a distant planar surface than will more flexible chains. At shorter distances, a similar trend occurs, but for very different reasons. The effects are highlighted in the inset of the figure, which shows the h -dependence of the difference, $\Delta f \equiv f - f^*$, where f^* is a fit of $f(h)$ to a power-law function in the intermediate regime of h where this scaling holds. At low h , Δf deviates significantly from zero. In the case of a freely-jointed chain ($\kappa = 0$), Δf is negative and

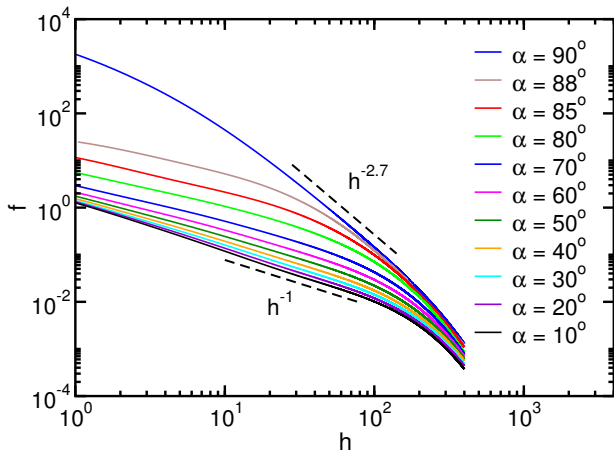


FIG. 9. Entropic force f vs tip-to-surface distance h for a polymer of length $N=5000$ and bending rigidity $\kappa = 4$. Results for different cone angles are shown. The dashed lines show the prediction of Eq. (6) ($f \sim h^{-1}$) as well as the prediction for slit confinement in the de Gennes regime ($f \sim h^{-2.7} \approx h^{-1/\nu-1}$).

decreases as h decreases. This deviation arises from violation of the condition that $a \ll h$ for Eq. (6) to be valid. Upon increasing κ , Δf also increases, becoming positive for $\kappa \gtrsim 4$. The physical origin of this trend is straightforward. A stiff polymer tethered to a cone tip close to the flat surface is forced to bend, giving rise to an appreciable bending energy and corresponding elastic force that pushes on the surface. This elastic force naturally increases with κ , giving rise to the observed trend at small h .

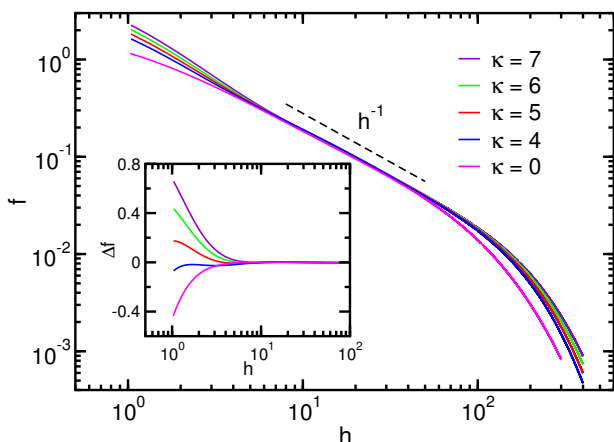


FIG. 10. Entropic force f vs tip-to-surface distance h for a polymer of length $N=5000$ and cone angle of $\alpha = 40^\circ$. Results for various values of the bending rigidity are shown. The inset shows the difference $\Delta f = f - f^*$ vs h , where $f^*(h)$ is the fit of each curve to the function $f^* = c_0 h^\mu$ in the range $h \in [8, 30]$.

C. Multiple tethered freely-jointed chains

We now consider the case of multiple polymers, each of length N and each tethered to the tip of the cone. This can also be viewed as a single star polymer with the branch point fixed to the cone tip, where the length of each arm is N . We denote the number of arms of the star polymer as n_{arm} . Figure 11 shows the variation of $\Delta F \equiv F(h=0) - F(h=\infty)$ with N . Results for a cone of angle $\alpha = 45^\circ$ and for a few different values of n_{arm} are shown. As in Figs. 2 and 7, ΔF varies with N as $F = a_0 + a_1 \ln N$ at sufficiently high N , consistent with the form of Eq. (2). Fitting each data set to this function yields an estimate for $\Delta\gamma$ from the fitting parameter a_1 . In Refs. 18 and 19, Maghrebi *et al.* used the ϵ -expansion to predict that

$$\frac{\mathcal{A}}{n_{\text{arm}}} = 1 - \frac{\epsilon}{8} + \left[\frac{3}{\pi} - \left(0.80 + \frac{11}{12\pi} (n_{\text{arm}} - 1) \right) \epsilon \right] \alpha^{1-3\epsilon/4}, \quad (14)$$

where $\mathcal{A} \equiv \Delta\gamma/\nu$ is the prefactor appearing in the force-distance relation of Eq. (3), and where $d - 3 = 1 - \epsilon$. Using $d = 3$ dimensions, and $\alpha = 45^\circ = \pi/4$ rad for the cone used in these calculations, it follows that

$$\frac{\mathcal{A}}{n_{\text{arm}}} \approx \text{const.} - \mathcal{B}n_{\text{arm}}, \quad (15)$$

where $\mathcal{B} = (11/12\pi)\alpha^{1/4}$. Thus, the theory predicts that the entropic force per arm *decreases* as the number of arms increases. For the cone used in these calculations, $\alpha = 45^\circ = \pi/4$ rad, yielding a value of $\mathcal{B} = 0.275$. To test this prediction, we plot $\mathcal{A}/n_{\text{arm}}$ vs n_{arm} in the inset of the figure, where $\mathcal{A} \equiv \Delta\gamma/\nu$, and where $\Delta\gamma$ are obtained from the fits described above. The results are shown in the inset of the figure. Consistent with the theoretical prediction, we find that $\mathcal{A}/n_{\text{arm}}$ does appear to decrease with increasing n_{arm} . However, the slope of the best linear fit is 0.053 ± 0.007 , which is about a factor of 5.2 smaller than the prediction for \mathcal{B} . For the case of cone angle $\alpha = 45^\circ$, the predicted force per arm decreases by roughly 10%.

Figure 12 shows the variation in the measured entropic force per arm with h for a star polymer of arm length $N = 1000$ with the branch point fixed to the tip of a cone of angle $\alpha = 45^\circ$. Results for a few values of n_{arm} are shown. The inset shows f vs h for the same data sets. As was the case for single tethered polymers, there is an intermediate range of h over which the relation $f = \mathcal{A}/h$ is approximately satisfied. A fit to each of the data sets in the range $h \in [3, 13]$ yields estimated exponents of -0.92 ± 0.04 , -0.94 ± 0.04 , -0.90 ± 0.02 , -0.91 ± 0.02 , and -0.95 ± 0.06 , for $n_{\text{arm}} = 1, 2, 3, 4$ and 5, respectively. Thus, as in previous cases, the scaling exponent differs slightly from the predicted value of -1 . Contrary to the prediction of Eq. (15) and the trend observed in Fig. 11, there is no clear evidence that the entropic force per arm decreases with n_{arm} . While it is possible

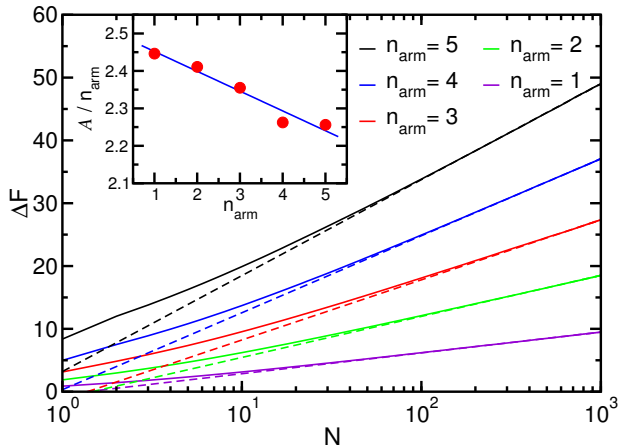


FIG. 11. Free energy difference, $\Delta F \equiv F(h=0) - F(h=\infty)$, for a star polymer with n_{arm} arms and with the branch point tethered to the tip of the cone. Results are shown for a cone angle of $\alpha = 45^\circ$ and a star polymer with the length of each arm up to $N = 1000$. Results are shown for $n_{\text{arm}} = 1-5$. The inset shows the variation of $\mathcal{A}/n_{\text{arm}}$ vs n_{arm} , where $\mathcal{A} \equiv \Delta\gamma/\nu$ and where $\Delta\gamma$ is obtained from the fit $\Delta F = \text{const} + \Delta\gamma N$ in the region $N \in [600, 1000]$. The blue line is a linear fit to the data.

that such an effect is masked by statistical limitations of the data, its magnitude is unlikely to be anywhere near to that predicted by the epsilon-expansion. Force-distance data generated from simulations using much longer chain lengths would be helpful to better elucidate this subtle effect, though this is not currently feasible. For the present, we tentatively conclude that total entropic force is simply proportional to the number of arms of a cone-tethered star polymer to an excellent approximation.

VI. CONCLUSIONS

In this study, we have used PERM MC simulations to characterize the entropic force between a hard conical surface and a hard planar surface mediated by one or more polymers tethered to the tip of the cone. These calculations were inspired by previous work by Maghrebi *et al.*,^{18,19} who predicted that the force should obey a scaling relation $f = \mathcal{A}k_B T/h$, where h is the cone-tip-to-surface distance. The relation is expected to hold for sufficiently long polymers in the regime $a \ll h \ll R_g$, where a is the polymer segment length and R_g is the radius of gyration for a free polymer. The prefactor is given by $\mathcal{A} = (\gamma_\infty - \gamma_0)/\nu$, where γ_∞ and γ_0 are critical exponents appearing in the partition function of the tethered polymer(s) and where ν is the Flory exponent for a self-avoiding polymer. We measured the force-distance relation for a single fully-flexible and semi-flexible cone-tethered hard-sphere chain, as well as a system with mul-

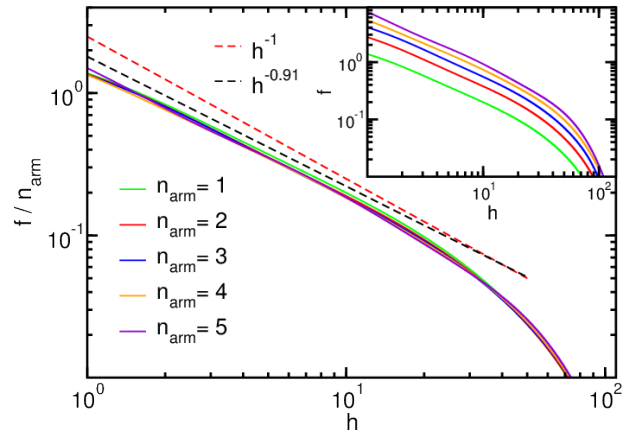


FIG. 12. Entropic force f per arm vs tip-to-surface distance h for a star polymer with n_{arm} arms and with the branch point tethered to the tip of the cone. Results are shown for an arm length $N=1000$ and cone angle of $\alpha = 45^\circ$. Results for various values of n_{arm} are shown. The inset shows f vs h for the same data sets.

tiple polymers end-tethered to the cone. In each case, we find that there is indeed an intermediate range of h for which the proportionality $f \propto h^{-1}$ approximately holds, though the scaling exponent tends to be somewhat smaller than the predicted value of 1. Simulations for $h = 0$ and $h = \infty$ facilitated calculation of the critical exponents γ_0 and γ_∞ and, thus, of the scaling prefactor \mathcal{A} . As in the case of the scaling exponent, we find the measured value of \mathcal{A} to be slightly smaller than the predicted value. These small discrepancies presumably arise from the various approximations employed in the analytical theory. On the other hand, within the valid range of h , the entropic force is independent of chain length and chain stiffness, and the scaling of the force with h is independent of the number of polymers tethered to the cone, all in accord with the prediction. In the case of multiple tethered polymers, we find that the entropic force scales proportional to the number of polymers, at least to within the precision of the calculations. This is in disagreement with the predictions from ϵ -expansion calculations carried out by Maghrebi *et al.*, in which the force per polymer is expected to *decrease* with the number of tethered polymers. Thus, this analytical method significantly overestimates any such effect.

As noted in Sec. I, the theoretical prediction of Maghrebi *et al.* has been tested in a recent AFM experiment by Liu *et al.*²⁰ Polyethylene glycol (PEG) polymers were tethered to a pyramidal AFM tip, and the force between the tip and a flat surface were measured as a function of the tip-to-surface distance. To measure the entropic force the van der Waals forces were eliminated by subtraction of the force measured in a separate experiment carried out with no polymers attached. Conditions were tuned to eliminate electrostatic forces and polymer

adhesion to the surface. In spite of these efforts, the theory provided a poor prediction for the observed trends, proving inferior to the predictions using the Alexander-de Gennes (AdG) theory for a confined polymer brush.²¹ An obvious source of the discrepancy arises from the structure of the AFM tip employed. In order to end-tether the PEG polymers, they were covalently bound to a well-defined Au patch at the apex of the cantilever tip, which had a surface area of about $3.7 \times 10^4 \text{ nm}^2$. On the other hand, the radius of gyration of the PEG molecules was only about 14 nm and 22 nm for the two different PEG molecular weights considered. Given these length scales, the system better resembles slit-confined surface-tethered polymers rather than the cone-plane-confined system described in Refs. 18 and 19 as well as the present study, thus accounting for the better agreement with the AdG theory. A better experimental test of the theory would require using much longer polymers or reducing the size of the patch at the cantilever tip apex. Even so, the truncation of the AFM tip to produce the patch introduces a new length scale that is expected to complicate the prediction that $f = \mathcal{A}k_B T/h$. In future work, we will use the computational methods employed here to quantify this effect. Another relevant feature to incorporate into the model is roughness of the planar surface (to which Liu *et al.* attribute anomalous behavior of the force at very low tip-to-surface distances). Measurements of the entropic force for such systems should be helpful for optimizing the design of future experiments to better test the theoretical prediction.

ACKNOWLEDGMENTS

This work was supported by the Natural Sciences and Engineering Research Council of Canada (NSERC) Discovery Grants Program. We are grateful to Compute Canada for use of their computational resources.

¹A. Cacciuto and E. Luijten, *Nano Lett.* **6**, 901 (2006).

²J. M. Polson, *J. Chem. Phys.* **142**, 174903 (2015).

³T. Sakaue, *J. Phys.: Condens. Matter* **30**, 244004 (2018).

- ⁴J. M. Polson and D. R. Heckbert, *Phys. Rev. E* **100**, 012504 (2019).
- ⁵L. Dai, C. B. Renner, and P. S. Doyle, *Adv. Colloid Interface Sci.* **232**, 80 (2016).
- ⁶E. Werner, G. K. Cheong, D. Gupta, K. D. Dorfman, and B. Mehlig, *Phys. Rev. Lett.* **119**, 268102 (2017).
- ⁷J. Z. Chen, *Phys. Rev. Lett.* **121**, 037801 (2018).
- ⁸J. M. Polson, A. F. Tremblett, and Z. R. McLure, *Macromolecules* **50**, 9515 (2017).
- ⁹J. M. Polson, *Macromolecules* **51**, 5962 (2018).
- ¹⁰L. Dai, J. J. Jones, J. R. van der Maarel, and P. S. Doyle, *Soft Matter* **8**, 2972 (2012).
- ¹¹N. Nikoofard, S. M. Hoseinpoor, and M. Zahedifar, *Phys. Rev. E* **90**, 062603 (2014).
- ¹²D. R. Tree, W. F. Reinhart, and K. D. Dorfman, *Macromolecules* **47**, 3672 (2014).
- ¹³G. K. Cheong, X. Li, and K. D. Dorfman, *Phys. Rev. E* **97**, 022502 (2018).
- ¹⁴Y. Teng, N. T. Andersen, and J. Z. Chen, *Macromolecules* **54**, 8008 (2021).
- ¹⁵A. R. Klotz, L. Duong, M. Mamaev, H. W. de Haan, J. Z. Chen, and W. W. Reisner, *Macromolecules* **48**, 5028 (2015).
- ¹⁶A. R. Klotz, M. Mamaev, L. Duong, H. W. de Haan, and W. W. Reisner, *Macromolecules* **48**, 4742 (2015).
- ¹⁷J. S. Leith, A. Kamanzi, D. Sean, D. Berard, A. C. Guthrie, C. M. McFaul, G. W. Slater, H. W. de Haan, and S. R. Leslie, *Macromolecules* **49**, 9266 (2016).
- ¹⁸M. F. Maghreb, Y. Kantor, and M. Kardar, *EPL* **96**, 66002 (2011).
- ¹⁹M. F. Maghreb, Y. Kantor, and M. Kardar, *Phys. Rev. E* **86**, 061801 (2012).
- ²⁰M. Liu, J. Xu, R. Zandi, and U. Mohideen, *J. Phys.: Condens. Matter* **31**, 075102 (2019).
- ²¹P. de Gennes, *Scaling Concepts in Polymer Physics* (Cornell University Press, Ithica NY, 1979).
- ²²M. Rubinstein and R. H. Colby, *Polymer Physics* (Oxford University Press, Oxford, 2003).
- ²³C. Micheletti, D. Marenduzzo, and E. Orlandini, *Phys. Rep.* **504**, 1 (2011).
- ²⁴D. R. Tree, A. Muralidhar, P. S. Doyle, and K. D. Dorfman, *Macromolecules* **46**, 8369 (2013).
- ²⁵T. Prellberg and J. Krawczyk, *Phys. Rev. Lett.* **92**, 120602 (2004).
- ²⁶P. Grassberger, *Phys. Rev. E* **56**, 3682 (1997).
- ²⁷H.-P. Hsu, W. Nadler, and P. Grassberger, *Macromolecules* **37**, 4658 (2004).
- ²⁸H.-P. Hsu and P. Grassberger, *EPL (Europhys. Lett.)* **66**, 874 (2004).
- ²⁹H.-P. Hsu and P. Grassberger, *J. Stat. Phys.* **144**, 597 (2011).
- ³⁰J. M. Polson and Z. R. McLure, *Phys. Rev. E* **99**, 062503 (2019).